Stem Cell Reviews and Reports (2022) 18:1127–1142
https://doi.org/10.1007/s12015-022-10327-x

Mesenchymal Stem Cell Derived Exosomes Suppress Neuronal Cell Ferroptosis Via lncGm36569/miR-5627-5p/FSP1 Axis in Acute Spinal Cord Injury

Chenglong Shao[1] · Yu Chen[2] · Tengyue Yang[1] · Haibiao Zhao[2] · Dongzhe Li[1]

Accepted: 1 January 2022 / Published online: 7 March 2022
© The Author(s), under exclusive licence to Springer Science+Business Media, LLC, part of Springer Nature 2022

Abstract

Exosomes derived from mesenchymal stem cells (MSCs) have been considered as an alternative for cell therapy of acute spinal cord injury (ASCI). However, the underlying mechanism remains unclear. Here, ASCI mouse model and hypoxic cell model were established to evaluate the effects of MSCs and MSCs-derived exosomes (MSCs-exo). The results showed that both MSCs and MSCs-exo inhibited the production of ROS and ferrous iron, upregulated the expression of ferroptosis suppressor FSP1, and enhanced repair of neurological function in the ASCI mice. Besides, MSCs and MSCs-exo attenuated hypoxia-induced neuronal cell ferroptosis and increased cell proliferation. Further study demonstrated that lncGm36569 was enriched in the MSCs-exo. Through bioinformatics analysis and luciferase assay, we confirmed that lncGm36569 acted as a competitive RNA of miR-5627-5p to induce FSP1 upregulation. Furthermore, overexpression of miR-5627-5p reversed the therapeutic effects of lncGm36569 on neuronal cell ferroptosis. In conclusion, MSCs-exosomes lncGm36569 inhibited neuronal cell ferroptosis through miR-5627-5p/FSP1 axis, thereby attenuating neuronal dysfunction.

Keywords Acute spinal cord injury · Mesenchymal stem cell · Exosome · lncGm36569 · miR-5627-5p · FSP1 · Ferroptosis

Abbreviation

MSCs	mesenchymal stem cells
ASCI	acute spinal cord injury
MSCs-Exo	mesenchymal stem cells derived exosomes
ROS	control is abbreviated as ctrl, reactive oxygen species
ACSL4	acyl-CoA synthetase 4
GPX4	glutathione peroxidase 4 expression
Nrf2	nuclear factor erythroid 2-related factor 2
BMS	Basso Mouse Scale
TEM	transmission electron microscope
MUT	mutant
WT	wildtype
AIFM2	apoptosis-inducing factor mitochondrial 2
ceRNAs	competing endogenous RNAs
CCK-8	Cell Counting Kit-8

✉ Dongzhe Li
ldz5056@126.com

Chenglong Shao
s290126156@163.com

[1] The Department of Orthopaedics, The First Affiliated Hospital of Zhengzhou University, Zhengzhou 450000, China

[2] The Department of Neurosurgery, The First Affiliated Hospital of Zhengzhou University, Zhengzhou 450000, China

Introduction

Acute spinal cord injury (ASCI) is a neural event with high mortality. ASCI commonly results in motor and sensory failures in patients, which causes great individual and societal burden [1, 2]. To date, it has been demonstrated that ASCI is not only triggered by the initial disruption of neuronal axons, blood vessels, and cell membranes. Systematical secondary injury induced by inflammatory, ischemia, hypoxia and progressive compression will also exacerbate ASCI, which rank the leading causes of neuronal cell death [3–5]. Therefore, understanding the molecular mechanism of neuronal cell death in ASCI is still in urgent need.

It is well known that autophagy and apoptosis of neuronal cells could be stimulated by ASCI. Furthermore, ferroptosis has been reported to be involved in the progression of ASCI. Ferroptosis is a novel form of iron-dependent programmed cell death characterized by increased reactive oxygen species (ROS) and lipid peroxidation

[6–10]. Chronic ASCI causes free radical accumulation, iron-catalyzed lipid peroxidation and iron overload at the injury site, consequently initiating ferroptosis [11–14]. Obvious changes of the redox and ferroptosis markers could also be observed in ASCI models in vivo, where acyl-CoA synthetase long-chain fatty acyl-CoA synthetase 4 (ACSL4) was up-regulated while glutathione peroxidase 4 (GPX4), nuclear factor erythroid 2-related factor 2 (Nrf2), and heme oxygenase-1 were down-regulated [15]. Some ferroptosis-related genes, such as Acyl-CoA synthetase family member 2 (ACSF2) and iron-responsive element-binding protein 2 (IREB2) were also down-regulated under spinal cord injury (SCI). Treatment with deferoxamine improved the repair of neuronal injury via suppressing ferroptosis [16]. Although these findings have provided important validation of ferroptosis as a potential target during ASCI repair, it is still necessary to illuminate the underlying mechanism and discover the effective reagents for ASCI therapy.

Currently, mesenchymal stem cells (MSCs) transplantation has a positive function on regulating behavioral outcome and histopathological assessment in spinal cord injured rats or patients [17–19]. MSCs therapy is considered as one promising approach to inhibit neuronal cell death and increase astrogliosis after ASCI [20, 21]. Exosomes derived from MSCs (MSCs-exo) are proved to possess great proangiogenic ability and are capable of inhibiting neuronal cell apoptosis to repair neural functions after traumatic SCI [22]. Moreover, MSCs derived exosomes maintained anti-scarring and anti-inflammatory effects, which also benefits ASCI treatment [23, 24]. Therefore, we believe that exosomes released by MSCs could be employed as an alternative therapy for SCI and may enhance the ASCI recovery.

Exosomes are one kind of extracellular vesicle with diameters of 50–200 nm and could be released by all type of cells. They participate in cell-cell communication by transferring the specific features, including lipids, proteins, and functional nucleic acid from the original cells into the recipient cells [25, 26]. Long non-coding RNAs (lncRNAs) are a crucial class of exosomal contents with more than 200 nucleotides. Numerous data demonstrates that lncRNAs distribute in both nucleus and cytoplasm. Based on the intracellular location of lncRNAs, they exert critical functions in regulating many biological processes, such as cell survival, differentiation and death through different molecular mechanism [27]. Researchers have revealed that lncRNAs are critical for regulating ferroptosis in many diseases through serving as competitive endogenous RNAs (ceRNAs) for microRNAs (miRNAs) [28–31]. However, the exact role of exosomal lncRNAs on ASCI-induced ferroptosis of neurons has not been discovered.

In this study, we identified that MSCs-derived exosomes had the potential to reduce neuronal ferroptosis and promote functional recovery in the ASCI model for the first time. Moreover, we revealed the role of lncGm36569/miR-5627-5p/FSP1 axis in ASCI progression. Our work provided a novel therapeutic target for ASCI.

Methods

Animal

Male C57BL/6 (7–8 weeks) were purchased from the Animal Center of Nanjing University (Nanjing, China) and housed in the condition with controlled temperature and humidity under a 12-h light/dark circadian rhythm. The animals were provided with food and water ad libitum. For determining the effects of MSCs-exo, the animals were derived into three groups: sham (n = 10), ASCI (n = 10), ASCI + MSCs (n = 10); for determining the effects of exosomal lncGm36569, the animals were divided into five groups: sham (n = 10), ASCI (n = 10), ASCI + MSC-Exo (ctrl) (n = 10), ASCI + MSCs-Exo (lnc-OE) (n = 10), ASCI + MSCs-Exo (si-lnc) (n = 10). The animal experiments were approved by the Animal Ethics Committee of The First Affiliated Hospital of Zhengzhou University.

Acute Spinal Cord Injury (ASCI) Model and Treatment

The ASCI model was constructed using Allen's method with some modifications [32]. After anesthetized by intraperitoneal injection of 4% chloral hydrate (3 ml/kg, Sinopharm group Co., Shanghai, China), the back of the mouse was opened to expose the T10 vertebral laminae and underwent dorsal laminectomy. Contusion was then induced by NYU Impactor M-III falling from the height of 3.0 cm. The sham mice underwent the same operation without contusion. Finally, the muscles and skin were sutured. Involuntary spasms in the hind limbs and wriggled tails of the mice indicated a successful ASCI model. After surgery, the mice were injected with cefuroxime sodium for 3 days to prevent infection and bladder evacuation was applied twice a day until the end of the study period. In the sham group, rats received only laminectomy. Three days after injury, the ASCI mice were subjected to MSCs transplantation or MSCs-exo treatment [33, 34]. MSCs or MSCs-exo (including MSCs-exo (ctrl), MSCs-exo (si-lnc), MSCs-exo (lnc-OE)) were resuspended in 3 μL of PBS and injected into the injured hind limbs. The sham mice were injected with the same volume of PBS without exosomes or MSCs. At the end of the experiment, the mice were euthanized with isoflurane

(5% for induction and 1.5% for maintenance) using a RWD R550 small animal anesthesia machine, followed by cervical dislocation, and the spinal cord tissues were removed for further analysis.

Behavioral Function Tests

Three evaluations were performed to assess the behavioral function, including locomotor performance evaluation, motor function evaluation, and sensory-motor function evaluation. All tests were performed 1, 3, 7, 14, 21, 28, 35, and 42 day(s) after modeling at the same time. The mice were allowed to rest for 30 min between different tests [35].

Briefly, locomotor performance was determined according to Basso Mouse Scale (BMS) [36]. The scores were evaluated according to the BMS-locomotion scale ranging from 0 to 9. A score of zero indicated for no observable locomotion while nice indicated normal locomotor activity. On each scoring day, the mice were individually placed in an open field (36 cm × 30 cm × 17 cm) and observed for 10 min. The mean scores obtained from two investigators were used for analysis Table 1.

The motor function was assessed by inclined plane test. In this test, each mouse was placed on an inclined plane, the largest angle that the mice could maintain its position for more than 5 s was recorded. Three trials were performed for each mouse and mean angle was used for analysis [37].

Beam walk test was applied to assess the sensory-motor function. Eight beams with different widths were designed to match the scoring scale (1–8). Each mouse was placed on the beams to walk from side to side. The narrowest beams that the mice could walk through without foot slip were recorded. Each mouse was tested for two times [38].

Cell Culture and Treatment

Mouse neuronal cell lines HT-22 and HEK-293 T were obtained from ATCC (Rockville, USA) and cultured in Dulbecco's modified Eagles medium (DMEM, Gibco, USA) containing 10% fetal bovine serum (FBS, Gibco, USA). Mouse bone marrow-derived MSCs were obtained from Cyagen Biosciences (Suzhou, China) and maintained in DMEM/F12 (Gibco, USA) supplemented with 10% FBS. To stimulate ASCI condition in vitro, HT-22 cells were exposed to hypoxic conditions (3% O_2, 5% CO_2 and 92% N_2) at 37 °C for 24 h. The control cells were maintained in normoxic conditions.

Co-Culture of MSCs and HT-22 Cells

HT-22 cells were plated in the lower chambers of the transwell system, whereas MSCs were plated in the upper chambers. GW4869 (20 μM, MedChemExpress, USA), a neutral sphingomyelinase inhibitor, was used to treat the MSCs cells for 48 h before co-culture to deplete exosomes in the co-culture system.

Western Blot

After different treatments, proteins from the cells or spinal cord tissues were collected using RIPA buffer. Equal

Table 1 Scores and operational definitions for the basso mouse scale for locomotion (BMS)

Score	standard of perfection
0	No ankle movement
1	Slight ankle movement
2	Extensive ankle movement
3	Plantar placing of the paw with or without weight support –OR Occasional, frequent or consistent dorsal stepping but no plantar stepping
4	Occasional plantar stepping
5	Frequent or consistent plantar stepping, no coordination –OR Frequent or consistent plantar stepping, some coordination, paws rotated at initial contact and lift off (R/R)
6	Frequent or consistent plantar stepping, some coordination, paws parallel at initial contact (P/R, P/P) -OR Frequent or consistent plantar stepping, mostly coordinated, paws rotated at initial contact and lift off (R/R)
7	Frequent or consistent plantar stepping, mostly coordinated, paws parallel at initial contact and rotated at lift off (P/R) -OR Frequent or consistent plantar stepping, mostly coordinated, paws parallel at initial contact and lift off (P/P), and severe trunk instability
8	Frequent or consistent plantar stepping, mostly coordinated, paws parallel at initial contact and lift off (P/P), and mild trunk instability -OR Frequent or consistent plantar stepping, mostly coordinated, paws parallel at initial contact and lift off (P/P), and normal trunk stability and tail down or up & down
9	Frequent or consistent plantar stepping, mostly coordinated, paws parallel at initial contact and lift off (P/P), and normal trunk stability and tail always up.

total proteins (30 μg/lane) were separated using 10% SDS-PAGE (Bio-Rad, USA) followed by transferring onto the PVDF membrane. After blocked with 5% BSA for 2 h at room temperature, the membranes were incubated with primary antibodies against FSP1(1:1000, Abcam, USA), GPX4 (1:1000, Abcam, USA), FTH1 (1:1000, Abcam, USA), NRF2 (1:1000, Abcam, USA), ACSL4 (1:1000, Abcam, USA), COX2 (1:1000, Abcam, USA), CD9 (1:1000, Abcam, USA), CD81 (1:1000, Abcam, USA), CD63 (1:1000, Abcam, USA), TSG101 (1:1000, Abcam, USA), and GAPDH (1:5000, Abcam, USA) at 4 °C overnight. Next, the membranes were incubated with HRP-conjugated secondary antibodies (1:5000, Abcam, USA) for 2 h at room temperature. The bands were then developed using enhanced chemiluminescence chromogenic substrate (GE Healthcare, UK) and analyzed by Image J software. GAPDH was used as a control in this study.

qRT-PCR

Total RNAs were extracted by TRIzol reagent (Thermo, USA) following the manufacturer's protocol. 1 μg of total RNA was revere-transcribed into cDNA using TaqMan Reverse Transcription Kit or TaqMan microRNA Reverse Transcription Kit (Applied Biosystems, USA). Next, cDNA was analyzed by the qRT-PCR system using SYBR green (Toyobo, Japan). The gene expression levels were calculated using the $2^{-\Delta\Delta CT}$ method and normalized by U6 or GAPDH. The primers used in this study were presented as follows: AIFM2 (mouse): forward 5'-CAACGGGGCTCTGAAAGTGA-3′, reverse 5'-AGCCTTCCGTGAGTCTAATCC-3′; GAPDH (mouse): forward 5'-TGAGGACCAGGTTGTCTCCT-3′, reverse 5'-GAGGGCACCAAACCTTCAGTT-3′; lncGm9725 (mouse): forward 5'-GGTGGGCAGTTAAAAGTCGC-3′, reverse 5'-ACAACATGCTGCAATGCTCTC-3′; lncGm14586 (mouse): forward 5'-CCAAGACCGTGAAGAAGGCT-3′, reverse 5'-TCTCACAGGCCCTCTCTGAA-3′; lncGm8623 (mouse): forward 5'-CCCCTGGAGATGATCGTGCG-3′, reverse 5'ACACGGACCCGAATATCCACAC-3′; lncGm36569 (mouse): forward 5'-TCATTTCTCTGCCGCTTCCA-3′, reverse 5'-AAAGAGCTCCTGTTTTCTGTACC-3′; mmu-miR-5627-5p: forward 5'-AGAGGGTGCGCCGGGC-3′, reverse 5'-AGTGCAGGGTCCGAGGTATT-3′; mmu-miR-326-5p: forward 5'-GGGGCAGGGCCTTTGTG-3′, reverse 5'-AGTGCAGGGTCCGAGGTATT-3′; U6 (mouse): forward 5'-GCTCGCTTCGGCAGCACAT-3′, reverse 5'-ATGGAACGCTTCACGAAT-3′.

Isolation of Exosomes

For exosome isolation, the MSCs after different transfections were maintained in the DMEM/F12 medium supplemented with 10% exosome-free fetal bovine serum. The MSCs-conditioned medium was harvested after 48 h, and centrifuged at 300×g for 15 min, 2500×g for 30 min, and 100,000×g for 4 h at 4 °C. The pellets were collected and laid on top of a 30% sucrose/D_2O cushion, followed by ultracentrifugation at 100000×g for 1 h at 4 °C. Finally, the pellets were resuspended in 200 μL PBS for further study [39]. For the in vitro exosome treatment, HT-22 cells were incubated with 100 ng/mL MSCs-exosomes (in 100 μL PBS) for 24 h before hypoxic stimulation.

Identification and Labeling of MSCs-Derived Exosomes

The morphologic feature of exosomes was determined using a transmission electron microscope (TEM) as a previous study described [40]. Besides, NanoSight NS300 (NTA, Malvern Instruments, China) was performed to examine the size of the exosomes according to the manufacturer's instructions. The protein markers were detected by western blotting as described above. In addition, the exosomes were labeled using a PKH67 green fluorescent labeling kit (Sigma, USA) following the manufacture's protocol. After incubation with HT-22 cells for 6 h, the PKH67 signals were detected under the fluorescent microscope.

Cell Transfection

miR-5627-5p inhibitor, mimic, lncGm36569 overexpressed vector (lnc-OE), lncGm36569 siRNA (si-lnc) and the corresponding controls, were obtained from GenePharma (Shanghai, China). For the in vitro transfection, the cells were plated on the 6-well plate at the density of 10^6 cells per well. Next, the cells were transfected with these reagents (5 μg) using Lipofectamine 2000 following the manufacturer's instructions. After 48 h, the cells were used for further studies.

Cell Counting Kit-8 (CCK-8) Assay

After different treatments, HT-22 cells were plated on 96-well plates (5000 cells/well) and incubated with 10 μL of CCK-8 reagent (Dojindo, Japan) at 37 °C for 2 h. The optical densities were detected by a microplate reader (Bio-Tek, USA) at 450 nm.

Iron Assay

Spinal cord samples and cells were collected to determine the intracellular ferrous iron level using the iron assay kit (Abcam, USA). In brief, after homogenization, the samples were incubated with an iron reducer on ice for 30 min, followed by staining with the iron probe for 1 h. The content of iron was measured by the microplate reader at 593 nm.

Reactive Oxygen Species (ROS) Detection

The ROS levels of spinal cord samples or cells were measured by the OxiSelectIn Vitro ROS/RNS Assay Kit (Cell Biolabs, USA) coupled with flow cytometry following the manufacturer's instructions. The data was normalized by the ROS level in spinal cord tissues from sham mice or control cells.

RNA Sequencing

The MSCs-exo were collected and washed with PBS. Total RNA was extracted using TRIzol reagent (Invitrogen) and revere-transcribed into cDNA. Then, the sequencing library was generated using the Stranded RNA-Seq Library Prep Kit (Illumina, USA), and subjected to the Illumina HiSeq 4000 Sequencing System. The data were analyzed by fold change and p value.

RNA Pull-Down Assay

The biotinylated DNA probes were hybridized with lncGm36569 or corresponding antisense RNA (NC) using the Biotin RNA Labeling Mix (Roche, USA) and T7/SP6 RNA polymerase (Roche). After purification using the RNeasy Mini Kit (Qiagen, USA), the lncRNA- or NC-banded probes were then dissolved and incubated with streptavidin-coated magnetic beads (Sigma, USA) at 25 °C for 2 h. Then, probes-coated beads were incubated with cell lysis at 4 °C for 3 h. The bound RNAs were eluted and isolated for qRT-PCR analysis [41].

Luciferase Assay

The 3'-UTR of AIFM2 and lncGm36569 were cloned into the pmiR-RB-REPORT vector (Ribobio, China). The binding sites among AIFM2, lncGm36569 and miR-5627-5p were mutated using the site directed mutagenesis kit (NEB E0554, USA). 10^6 HEK-293 T cells were seeded on the 6-well plate and co-transfected with mutant (MUT)/wildtype (WT) vector and miR-5627-5p mimic/inhibitor or controls using Lipofectamine 3000 reagent (Ribobio, China). After 48 h, the luciferase activity was determined using a Dual-Luciferase Assay System (Promega, USA).

Elisa

The spinal cord tissues were homogenize in PBS and centrifuged at 3000 rpm to obtain the supernatant. Next, the supernatant was incubate with the 1x biotinylated detection antibody for 1 h followed by HRP-streptavidin solution for 45 min. The optical densities at 450 nm were recorded.

Statistical Analysis

Data were analyzed using the Prism 8.0 software and showed as means ± SD. Two-tailed Student's t test was used for comparisons between the two groups. One-way ANOVA was performed to compare the difference among multiple groups. $P < 0.05$ was considered as statistically significant.

Results

Functional Improvements in ASCI Mice Treated with MSCs

We first performed experiments to assess functional recovery for 6 weeks post-ASCI to evaluate the efficiency of MSC therapy. Firstly, we assessed the locomotor performance using BMS score. The results showed that the scores were significantly lower in ASCI mice than that of the sham group, and showed a slow upward trend with the post-ASCI days increasing. On the twenty-first day, MSCs markedly increased the BMS scores of ASCI mice, indicating the favorable therapeutic effects on motor function. Secondly, the beam walk test was performed and demonstrated that the injured mice exhibited severe disorder after ASCI operation, while this score was dramatically increased in the MSCs-treated group. Besides, the mean angle in the inclined plane test was about 80° for the sham mice, while ASCI decreased the angles. However, treated with MSCs continuously increased the angles and presented significant gains 4 weeks after injury (Fig. 1a). In addition, after ASCI, higher levels of ROS and intracellular ferrous iron accumulation were observed in the injured mice than the sham group, which were both reversed after MSCs treatment (Fig. 1b and c). Using the western blotting analysis, we found that the protein levels of GPX4, FTH1 and FSP1 were significantly decreased in the mice subjected to ASCI, while no significant changes were observed on the levels of other ferroptosis markers, including NRF2, ACSL4 and COX2. Notably, treating the ASCI mice with MSCs significantly re-upregulated the levels of GPX4, FTH1 and FSP1 (Fig. 1d). These findings suggested that FSP1-mediated ferroptosis suppression was inhibited following ASCI and MSCs exerted an effective therapeutic effect for ASCI in vivo.

MSCs Inhibited Neuronal Cell Ferroptosis In Vitro

To further confirm the effects of MSCs on FSP1-mediated ferroptosis, HT-22 cells were co-cultured with MSCs for 24 h under hypoxia stimulation. The results

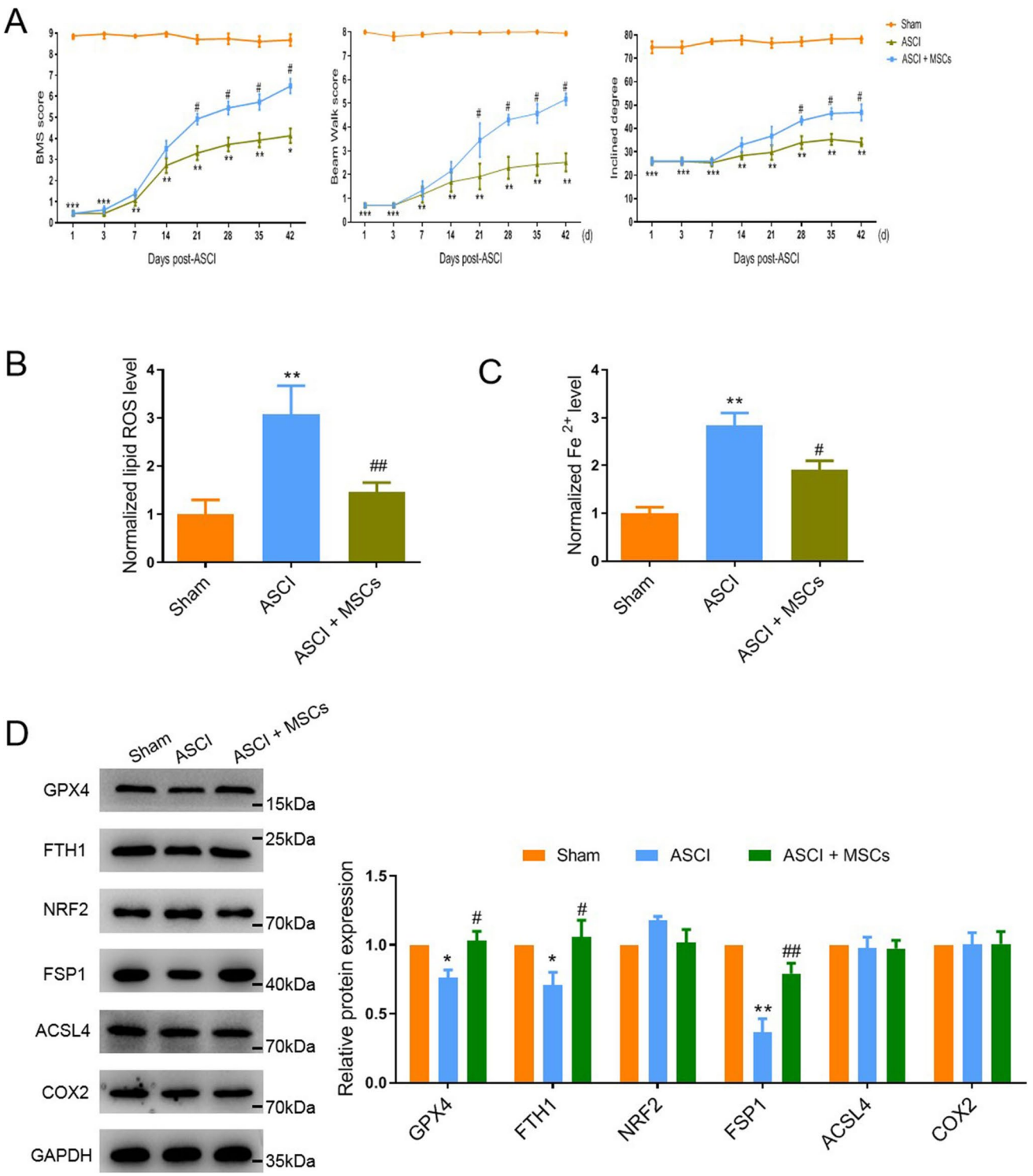

Fig. 1 MSCs improved neurological function and inhibited FSP1-mediated ferroptosis in ASCI mice. ASCI mouse model was established and treated by MSCs. **a** The functional disorder of the ASCI model with or without MSCs treatment was assessed using BMS score, beam walk score, and inclined angle. **b** and **c** The accumulations of lipid ROS and ferries iron in the injured spinal cord tissues were determined. **d** Western blotting analysis was performed for the expression levels of ferroptosis markers, including GPX4, FTH1, NRF2, FSP1, ACSL4, and COX2 in the spinal cord tissues from ASCI mice, and the representative blot images were displayed. The mice were equally divided into each group (n = 10), *p < 0.05, **p < 0.01, ***p < 0.001 vs. the sham group; #p < 0.05, ##p < 0.01 vs. the ASCI group

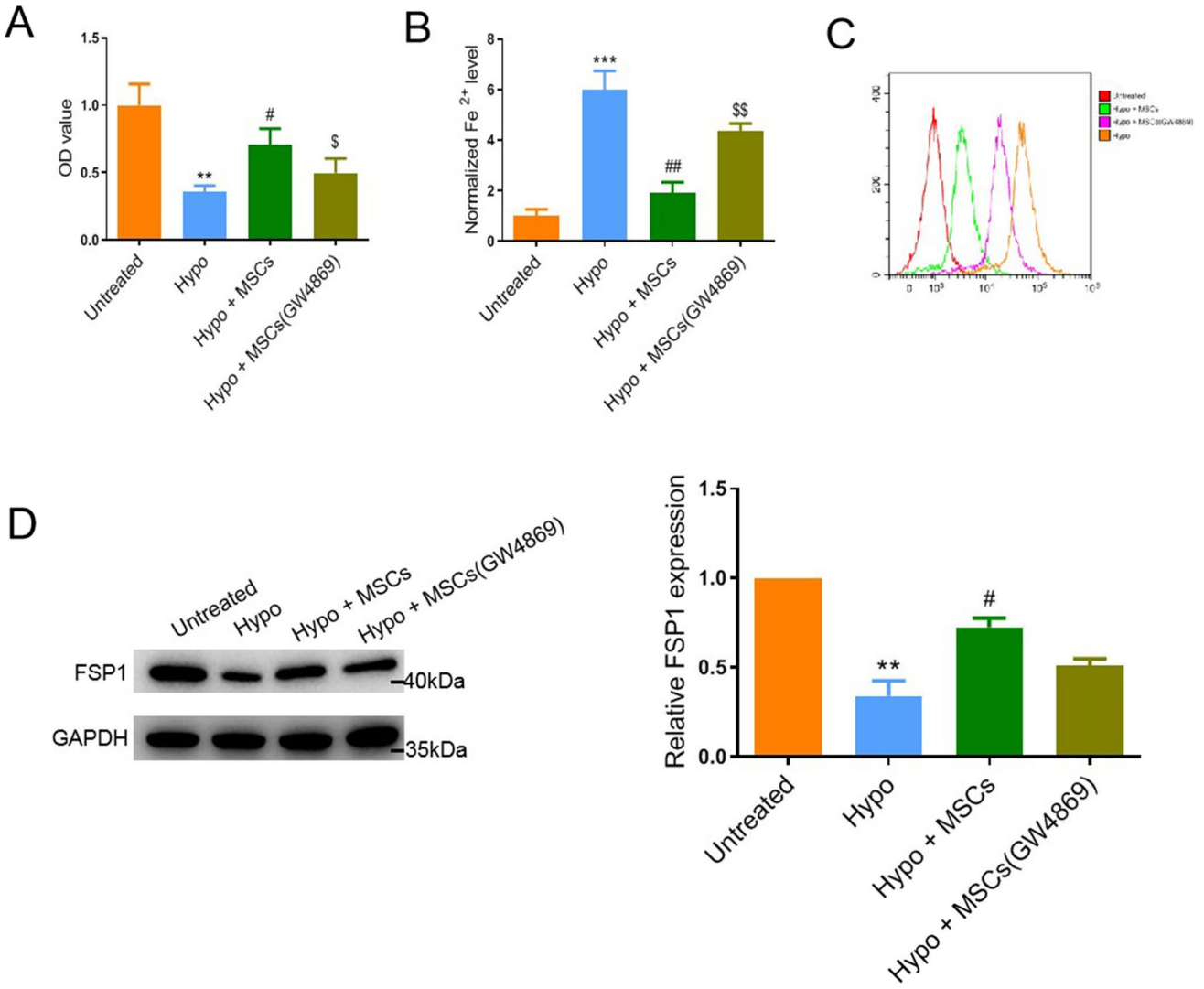

Fig. 2 MSCs enhanced neuronal cell proliferation and inhibited FSP1-mediated ferroptosis. The neuronal cells were exposed to hypoxic condition and co-cultured with MSCs or GW4869-treated MSCs. **a** Cell viability was assessed using CCK-8 assay. **b** and **c** The ferrous iron (Fe^{2+}) and ROS levels in the neuronal cells were detected by iron assay and flow cytometry, respectively. **d** The relative protein levels of FSP1 were examined by western blot, GAPDH acted as the control. Data were expressed as mean ± SD, n = 3, **p < 0.01, ***p < 0.001 vs. the untreated group; #p < 0.05, ##p < 0.01 vs. the hypoxia group; $p < 0.05, $$ < 0.01 vs. the Hypo + MSCs group. Hypo, hypoxia

demonstrated that hypoxia exposure markedly reduced cell viability (Fig. 2a) and significantly upregulated iron and ROS production in neuronal cells (Fig. 2b and c). Besides, western blotting analysis showed that compared with the untreated group, a decreased protein level of FSP1 was detected in the neuronal cells (Fig. 2d). However, these phenomena were abolished after co-culturing with MSCs (Fig. 2). Interestingly, when we treated MSCs with GW4869 prior to co-culture, the effects of MSCs were significantly reversed (Fig. 2). Thus, we aimed to investigate whether the functions of MSCs were caused by the endogenous exosomes.

MSCs-Exo Inhibited Cell Ferroptosis under the Hypoxic Condition

For this purpose, exosomes derived from MSCs were isolated by ultra-centrifugation, and confirmed using transmission electron microscope (TEM) and NanoSight NS300 (NTA). As shown in Fig. 3a to c, MSCs-exo presented round structures with diameters about 50 nm to 200 nm, and four positive exosome markers, CD63, CD81, CD9, and TSG101, were all detected in these vesicles. Besides, we observed that these exosomes could be uptake by HT-22 cells,

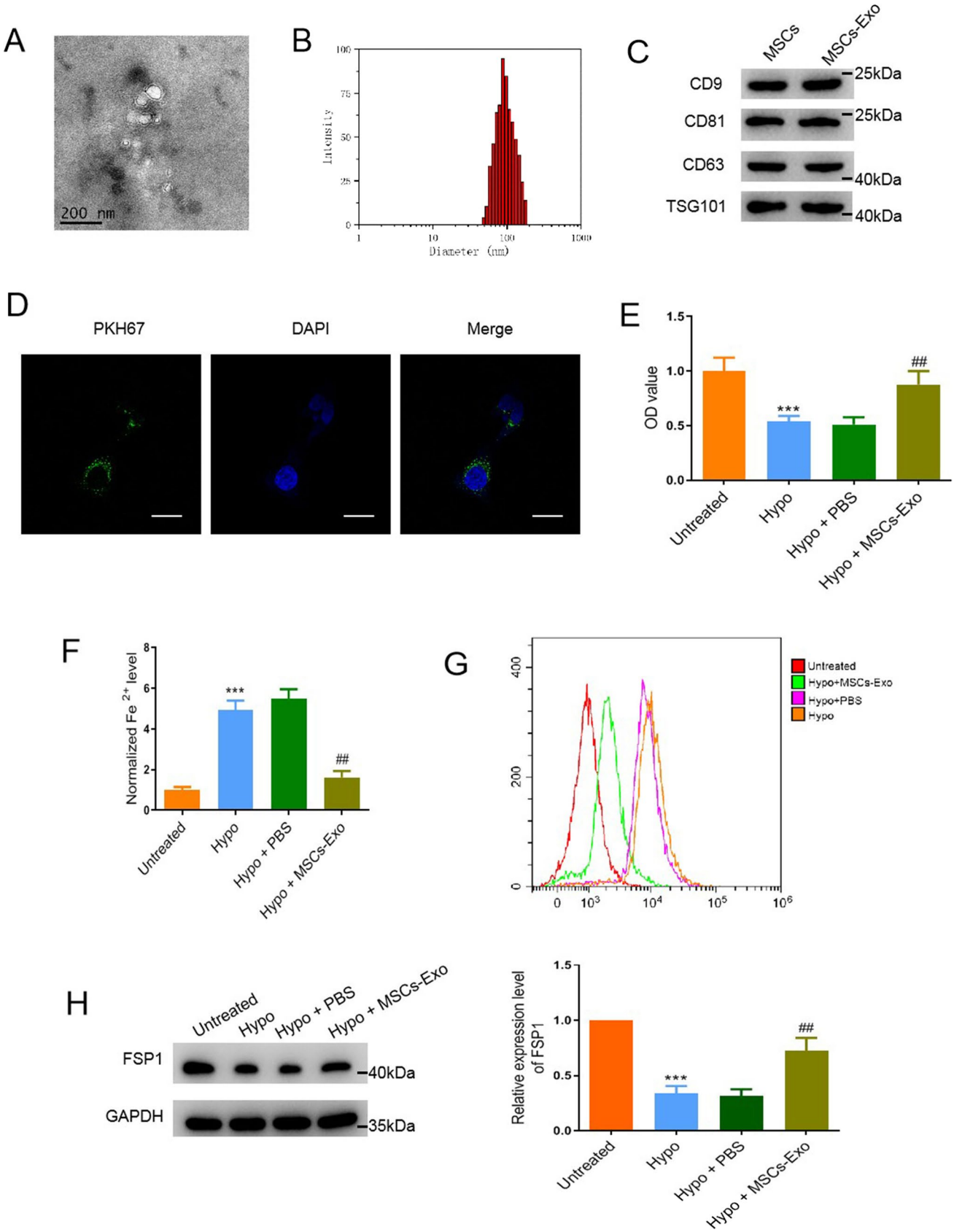
A
200 nm
B
Intensity
Diameter (nm)
C
MSCs
MSCs-Exo
CD9
CD81
CD63
TSG101
25kDa
25kDa
40kDa
40kDa
D
PKH67
DAPI
Merge
E
OD value
Untreated
Hypo
Hypo + PBS
Hypo + MSCs-Exo
F
Normalized Fe 2+ level
G
Untreated
Hypo+MSCs-Exo
Hypo+PBS
Hypo
H
FSP1
GAPDH
40kDa
35kDa
Relative expression level of FSP1

◂**Fig. 3 MSCs-exo inhibited cell ferroptosis under the hypoxic condition**. Exosomes were isolated from the mouse bone marrow-derived MSCs. **a** The morphology of MSCs-exo was observed by a transmission electron microscope. Bar = 200 nm. **b** The particle sizes of exosomes were assessed by NTA. **c** Western blot assay was performed for the expression levels of exosome positive markers, including CD9, CD81, CD63 and TSG101 in the MSCs and MSCs-exosomes. **d** Immunofluorescence assay revealed that MSCs-exo could be uptake by HT-22 cells. Bar = 20 μm. **E.** Cell viabilities of neuronal cells after PBS or MSCs-exo treatment under hypoxic conditions were examined by CCK-8 assay. **f** and **g** The ferrous iron (Fe^{2+}) and ROS levels in the hypoxia-exposed cells after different treatments was detected by iron assay kit and flow cytometry, respectively. **h** The relative protein levels of FSP1 were examined by western blot, GAPDH acted as the control. Data were expressed as mean ± SD, n = 3, ***p < 0.001 vs. the untreated group; ##p < 0.01 vs. the hypoxia group. Hypo, hypoxia; MSCs-Exo, MSCs-derived exosomes

as evidenced by clear green signals (PKH67) inside HT-22 cells. PKH67-labeled exosomes were observed to mainly locate in the cytoplasm of HT-22 cells, indicating that the exosomes can be successfully swallowed into the cytoplasm of HT-22 cells (Fig. 3d). Compared with the PBS-treated group, MSCs-exo significantly increased cell viability reduced by hypoxia exposure (Fig. 3e). Consistently, the levels of ROS and iron were both significantly upregulated in the cells exposed to hypoxic conditions. No notable change was detected in these hallmarks of ferroptosis following PBS treatment. Nevertheless, MSCs-exo administration led to a dramatic decrease in these markers (Fig. 3f and g). The protein levels of FSP1 were decreased in the cells under hypoxic conditions and the decrement could be reversed by exosomes (Fig. 3h).

LncGm36569 Was Enriched in MSCs-Exo and Associated with the FSP1-Mediated Ferroptosis In Vitro

Next, we compared the lncRNA profiles between HEK293T cells and MSCs derived exosomes. As shown in Fig. 4a, there was a total of 1148 differentially expressed lncRNAs, among which 642 lncRNAs were upregulated and 506 lncRNAs were downregulated. The top four lncRNAs, including lncGM9725, lncGM14586, lncGM8623 and lncGm36569, were chosen and confirmed by qRT-PCR. Among them, the level of lncGm36569 was elevated about 10-fold in the MSCs-exosomes than the control group (Fig. 4b). QPCR also showed that lncGm36569 was highly enriched in the MSCs-exosomes, and after overexpression of lncGm36569, the expression level of lncGm36569 increased significantly. It showed that overexpression of lncGm36569 and MSCs-exosomes had similar therapeutic effects (Fig. 4c). Moreover, overexpression of lncGm36569 in hypoxia exposed cells significantly suppressed ferroptosis-mediated cell death via downregulating iron and ROS accumulation. Besides, the expression level of FSP1 was notably upregulated by lncGm36569. Oppositely, inhibition of lncGm36569 promoted the productions of iron and ROS but decreased FSP1 expression (Fig. 4d-g). These results indicated that lncGm36569 played a key role in hypoxia-induced ferroptosis.

LncGm36569 Acted as a ceRNA of miR-5627-5p to Increase the Level of FSP1

One previous study reported that lncRNAs could regulate the development of ASCI by acting as ceRNAs of miRNAs [42]. We designed to identify whether the neuroprotective effects of lncGm36569 were achieved through regulating miRNAs. To assess this hypothesis, an online bioinformatics database (miRanda, www.miranda.org) was used to predict the target miRNAs of lncGm36569 following the prediction score and free-energy. We found that 38 miRNAs had strong binding potential with lncGm36569. Moreover, miRDB (www.mirdb.org) and miWalk (www.mirwalk.umm.uni-heidelberg.de) were employed to figure out the miRNAs targeted for FSP1. Finally, two overlapping miRNAs of all three databases, miR-326-5p and miR-5627-5p, were chosen and examined by qRT-PCR analysis and biotin-labeled pull-down assay. The results showed that compared with the control group, lncGm36569-coated pellets enriched both miR-5627-5p and miR-326-5p. However, the enrichment of miR-5627-5p was significantly higher than that of miR-326-5p (Fig. 5a and b). Hence, miR-5627-5p was selected for the subsequent experiments. To identify the role of lncGm36569, gain- and loss-of-function experiments were performed. The results showed that overexpression of lncGm36569 markedly inhibited the expression level of miR-5627-5p, whereas silencing of lncGm36569 increased the level of miR-5627-5p by about six times compared to the control group (Fig. 5c). As shown in Fig. 5d, the binding site was predicted by RNAhybird database (www.bibiserv.cebitec.uni-bielefeld.de/rnahybrid). Based on luciferase reporter assay, we identified that luciferase activity in the cells transfected with wild type 3'-UTR of lncGm36569 was significantly reduced by miR-5627-5p mimic, while the luciferase activity

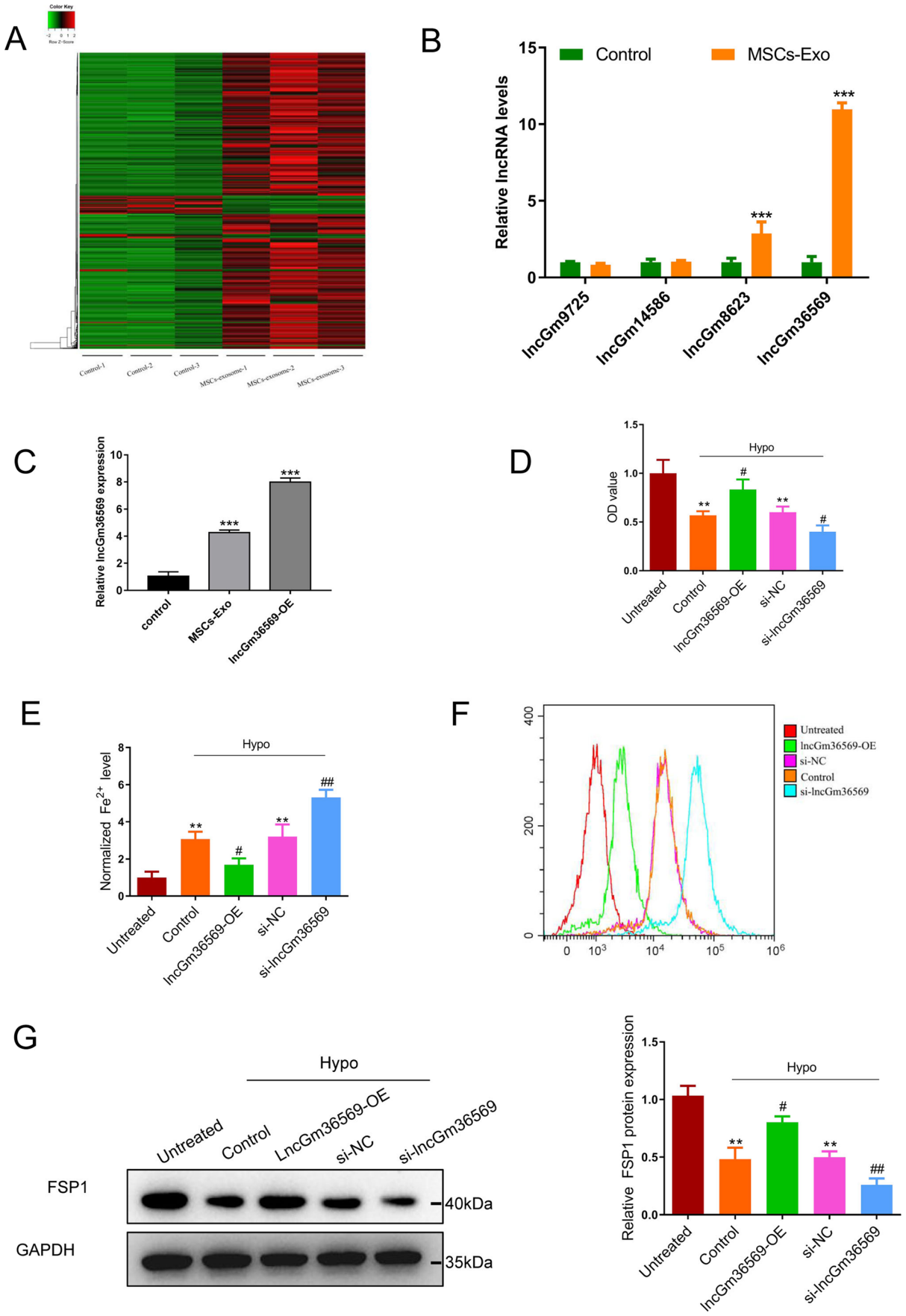
A
Color Key
Control-1
Control-2
Control-3
MSCs-exosome-1
MSCs-exosome-2
MSCs-exosome-3
B
Control
MSCs-Exo
Relative lncRNA levels
lncGm9725
lncGm14586
lncGm8623
lncGm36569
C
Relative lncGm36569 expression
control
MSCs-Exo
lncGm36569-OE
D
Hypo
OD value
Untreated
Control
lncGm36569-OE
si-NC
si-lncGm36569
E
Hypo
Normalized Fe2+ level
Untreated
Control
lncGm36569-OE
si-NC
si-lncGm36569
F
Untreated
lncGm36569-OE
si-NC
Control
si-lncGm36569
G
Hypo
Untreated
Control
LncGm36569-OE
si-NC
si-lncGm36569
FSP1
GAPDH
40kDa
35kDa
Relative FSP1 protein expression

◂**Fig. 4 LncGm36569 was upregulated in MSCs-exo and contributed to amelioration of ferroptosis**. **a** Hierarchical clustering analysis of differentially expressed lncRNAs between HEK293 cell derived exosomes and MSCs-exo, llog fold changel >2 and P < 0.05 were applied to filter the lncRNAs. Expression values showed in red color indicated the upregulated lncRNAs, and green color represented the downregulated lncRNAs. **b** Real-time PCR analysis of the top four increased lncRNAs in the exosomes from the MSCs. ***p < 0.001 vs. the control group. **c** QPCR analysis of lncGm36569 in the MSCs-exosomes. ***p < 0.001 vs. the control group. **d**, **e** and **f** The neuronal cells were transfected with lncGm36569 overexpression vectors or si-lncGm36569 prior to hypoxia exposure. Cell viability, ferrous iron and ROS accumulations were determined using CCK-8, iron assay and flow cytometry, respectively. **g** Western blot assay was performed for the expression levels of FSP1 in the neuronal cells after different transfections. Data were expressed as mean ± SD, n = 3, **p < 0.01 vs. the untreated group; #p < 0.05, ##p < 0.01 vs. the vector group or the si-NC group. Hypo, hypoxia; OE, overexpression; NC, negative control

was markedly upregulated after miR-5627-5p inhibitor transfection (Fig. 5e). Furthermore, bioinformatics analysis showed that FSP1 3'-UTR harbored binding sites for miR-5627-5p (Fig. 5f). To confirm the relationship between miR-5627-5p and FSP1, luciferase reporter assay was performed. As shown in Fig. 5g, overexpression of miR-5627-5p dramatically decreased the luciferase activity of wildtype FSP1, while inhibition of miRNA using inhibitor increased the level. However, cells co-transfected with mutant FSP1 3'-UTR and miRNA mimic or inhibitor presented no changes in the luciferase activity.

Next, we investigated the role of lncGm36569/miR-5627-5p/FSP1 axis in regulating hypoxia-induced ferroptosis in vitro. Compared to the control group, lncGm36569 overexpression reversed the reduction of cell viability induced by hypoxia exposure, with a notable decline of ROS and iron, as well as a significant upregulation of FSP1. However, overexpression of miR-5627-5p partly enhanced the effect of hypoxia on cell viability, production of iron and ROS, and inhibited the expression of FSP1. Co-transfection with miR-5627-5p mimic significantly reversed the protective effect of lncGm36569-OE vector in hypoxia exposed HT-22 cells (Fig. 5h-k). These findings suggested that lncGm36569 might sponge miR-5627-5p to inhibit FSP1-mediated ferroptosis in neuronal cells.

Exosomal lncGm36569 Improved Functional Disorder In Vivo Via miR-5627-5p/FSP1 Axis

We next investigated whether exosomal lncGm36569 exhibited therapeutic effects on ASCI. BMS score was significantly increased in the ASCI mice after MSCs-exosome (ctrl) or MSCs-exosomes (lnc-OE) treatment. At the end of the period, overexpression of lncGm36569 presented higher behavior score than the control exosome-treated group, but no significant difference was observed between ctrl and lnc-OE groups; knockdown of lncGm36569 notably decreased BMS score of the ASCI mice compared to the ctrl group (Fig. 6a, left). Lnc-OE and si-lnc showed the similar effects on beam walk score with BMS score; however, lnc-OE group showed little amelioration on beam walking compared to ctrl group (Fig. 6a, right). In addition, western blotting analysis and IHC analysis revealed that MSCs-exosomes (ctrl) upregulated FSP1 expression. Interestingly, overexpression of lncGm36569 in these exosomes further enhanced the FSP1 expression level (Fig. 6b). ASCI group exhibited a more serious inflammation status compared with the sham group, as evidenced by increased levels of IL-1β and IL-6. MSCs-exosome(ctrl) or MSCs-exosomes (lnc-OE) treatment decreased the levels of these inflammatory factors, while knockdown of lncGm36569 increased the levels (Fig. 6c). lncGm36569 overexpression exosomes inhibited miR-5627-5p expression in the ASCI model, whereas lncGm36569-depleted exosomes increased the level of miR-5627-5p (Fig. 6d). These findings indicated that exosomal lncGm36569 alleviated FSP1-mediated ferroptosis after ASCI via miR-5627-5p/FSP1 axis.

Discussion

Promoting viability of neuronal cells is considered as a strategic approach to improve the functional disorder after ASCI. In this study, we demonstrated that MSCs and the derived exosomes enhanced neuronal cell growth and inhibited ferroptosis-induced cell death. Besides, we found that the therapeutic effects of MSCs-derived exosomes relied on a novel lncRNA Gm36569, which served as a competitive endogenous RNA (ceRNA) of miR-5627-5p to enhance FSP1 expression, consequently suppressing ferroptosis in injured neuronal cells.

Ferroptosis is an essential form of neuronal cell death under ischemia/hypoxic condition, which may cause secondary injury after ASCI. The main regulatory mechanisms involved in ferroptosis are iron ion metabolism, antioxidant system and lipid metabolism [43]. GPX4 is a key enzyme that hydrolyzes lipid peroxides in vivo. Inhibition of GPX4 can induce ferroptosis, and overexpression of GPX4 can help to reduce ferroptosis [14]. FSP1 is an effective ferroptosis resistance factor that acts

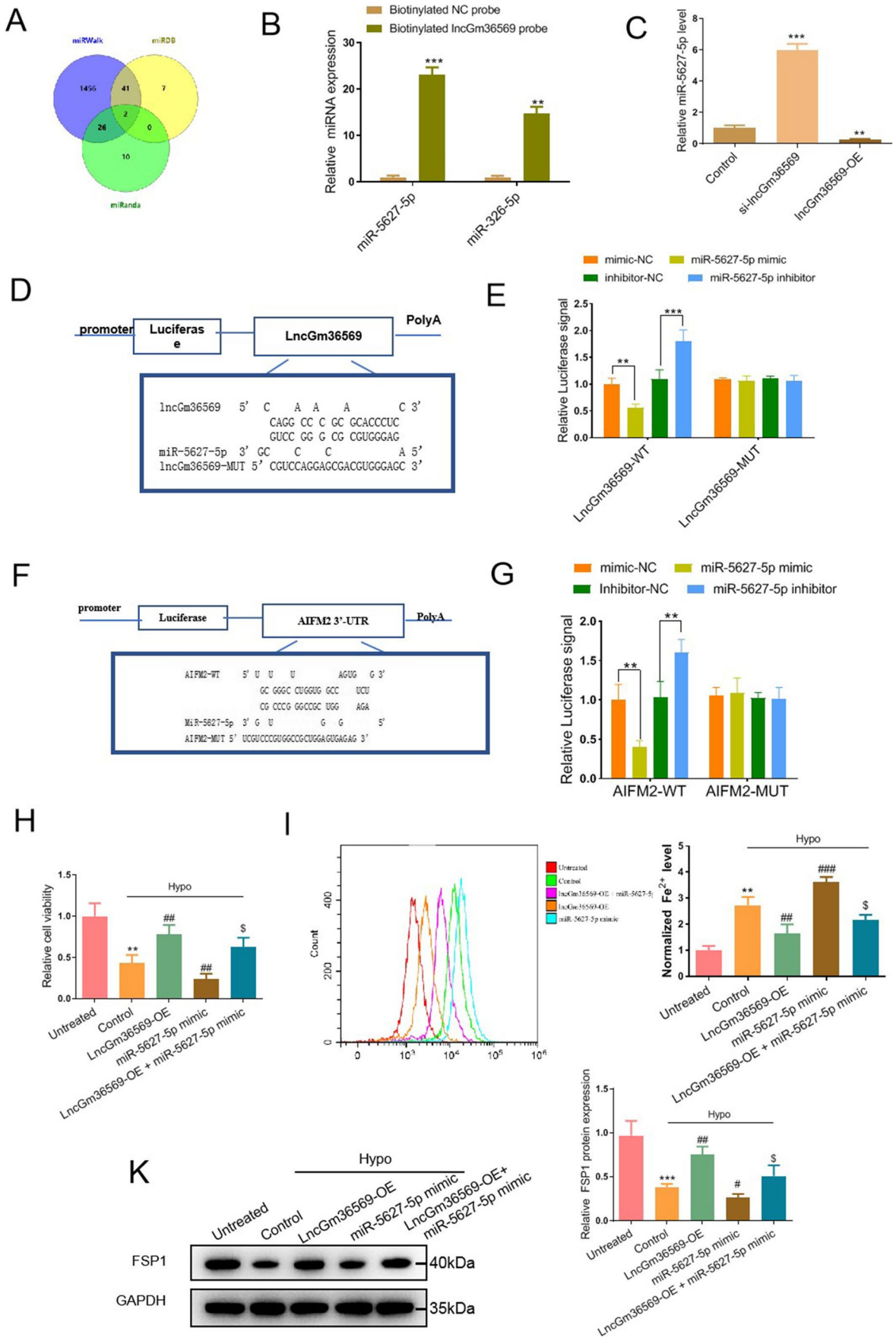
A
miRWalk
miRDB
miRanda
1456
41
7
2
26
0
10
B
Biotinylated NC probe
Biotinylated lncGm36569 probe
Relative miRNA expression
miR-5627-5p
miR-326-5p
C
Relative miR-5627-5p level
Control
si-lncGm36569
lncGm36569-OE
D
promoter
Luciferase
LncGm36569
PolyA
lncGm36569 5' C A A A C 3'
CAGG CC C GC GCACCCUC
GUCC GG G CG CGUGGGAG
miR-5627-5p 3' GC C C A 5'
lncGm36569-MUT 5' CGUCCAGGAGCGACGUGGGAGC 3'
E
mimic-NC
miR-5627-5p mimic
inhibitor-NC
miR-5627-5p inhibitor
Relative Luciferase signal
LncGm36569-WT
LncGm36569-MUT
F
promoter
Luciferase
AIFM2 3'-UTR
PolyA
AIFM2-WT 5' U U U AGUG G 3'
GC GGGC CUGGUG GCC UCU
CG CCCG GGCCGC UGG AGA
MiR-5627-5p 3' G U G G 5'
AIFM2-MUT 5' UCGUCCCGUGGCCGCUGGAGUGAGAG 3'
G
mimic-NC
miR-5627-5p mimic
Inhibitor-NC
miR-5627-5p inhibitor
Relative Luciferase signal
AIFM2-WT
AIFM2-MUT
H
Relative cell viability
Hypo
Untreated
Control
LncGm36569-OE
miR-5627-5p mimic
LncGm36569-OE + miR-5627-5p mimic
I
Count
Normalized Fe2+ level
Hypo
Untreated
Control
LncGm36569-OE
miR-5627-5p mimic
LncGm36569-OE + miR-5627-5p mimic
Relative FSP1 protein expression
Hypo
K
Hypo
Untreated
Control
LncGm36569-OE
miR-5627-5p mimic
LncGm36569-OE+ miR-5627-5p mimic
FSP1
40kDa
GAPDH
35kDa

◂**Fig. 5 lncGm36569 acted as a ceRNA of miR-5627-5p to increase FSP1 expression**. **a** The target miRNAs of lncGm36569 were predicted by miRanda database; miRNAs targeted for FSP1 were predicted by miRDB and miRWalk databases. The predicted miRNAs were presented in the Venn image and the overlapping miRNAs were selected for the subsequent experiments. **b** The expression levels of miR-5627-5p and miR-326-5p were assessed by qRT-PCR. $^{**}p<0.01$, $^{***}p<0.001$ vs. the biotinylated NC probe group. **c** Real-time PCR analysis was employed to measure the expression of miR-5627-5p in HT-22 cells with si-lncGm36569 or lncGm36569-OE transfection. $^{**}p<0.01$, $^{***}p<0.001$ vs. the control group. **d** The potential sequence of binding site between lncGm36569 and miR-5627-5p. **e** Luciferase activities were determined in HEK293T cells co-transfected with luciferase reporter containing wild/mutant type of lncGm36569 and miR-5627-5p mimic/inhibitor. Luciferase activity was normalized by renilla luciferase. $^{**}p<0.01$, $^{***}p<0.001$ vs. the mimic-NC or inhibitor-NC group. **f** The sequence of potential binding site between AIFM2 (FSP1) and miR-5627-5p. **g** Luciferase activities were determined in HEK293T cells co-transfected with luciferase reporter containing wild/mutant type of AIFM2 (FSP1) and miR-5627-5p mimic/inhibitor. Luciferase activity was normalized by renilla luciferase. $^{**}p<0.01$, $^{***}p<0.001$ vs. the mimic-NC or inhibitor-NC group. **h**, **i** and **j.** The neuronal cells were transfected with lncGm36569 overexpression vector or miR-5627-5p mimic prior to hypoxia exposure. Cell viability, ferrous iron and ROS accumulations were performed using CCK-8, iron assay and flow cytometry, respectively. **k** Western blot analysis was performed for the expression levels of FSP1 in the neuronal cells after different transfections, and representative blot images were displayed. Data were expressed as mean ± SD, n = 3, $^{**}p<0.01$, $^{***}p<0.001$ vs. the untreated group; $\#p<0.05$, $\#\#p<0.01$, $\#\#\#p<0.001$ vs. the control group; $\$p<0.05$ vs. the lncGm36569-OE group. Hypo, hypoxia; OE, overexpression; WT, wildtype; MUT, mutant

by recruiting a large amount of antioxidants to inhibit the excessive accumulation of lipid peroxides [44]. Besides, iron transport and circulation are inseparable from ferritin; hence, ferritin Heavy Chain 1 (FTH1) is vital in the process of iron metabolism [45]. In this study, we found that both ferrous iron and ROS levels were enhanced in the ASCI mice and the expression levels of GPX4, FTH1 and FSP1 were markedly decreased, suggesting that ferroptosis was initiated in the spinal cord tissues of ASCI mice. In addition, we detected other ferroptosis related proteins including NRF2, ACSL4 and COX2. ACSL4 is a lipid metabolism-related gene, which was previously reported to activate ferroptosis [46]. NRF2 is a master regulator of cytoprotective program against oxidative stress and it participates in the regulation of ferroptosis [47]. COX2 belongs to the cyclooxygenase family, which promotes ferroptosis by catalyzing the oxidation reaction of unsaturated fatty acids in membrane phospholipids [48]. Protein expressions of these three ferroptosis-related genes showed no significant change between the mice in ASCI and sham groups, indicating that ASCI was not associated with ACSL4, NRF2 and COX2 proteins. When neuronal cells were exposed to hypoxic conditions, similar changes of these ferroptosis hallmarks were observed. FSP1 is a glutathione-independent ferroptosis resistance factor and is encoded by apoptosis-inducing factor mitochondrial 2 (AIFM2). Also, it is an essential factor in the non-mitochondrial CoQ antioxidant system [49]. FSP1 has been revealed to contribute to neuroprotection [50]. Given this protection, we paid our attention to the changes of FSP1, and aimed to unveil the underlying mechanism of ASCI-induced ferroptosis mediated by FSP1.

To date, MSCs-derived exosomes have been reported to protect neuronal cells against apoptosis after ASCI. However, whether exosomes could regulate neuronal cell ferroptosis remains unknown. In the present work, we observed that MSCs-exo improved the functional defects and decreased the high levels of ROS and iron in ASCI mice. Furthermore, MSCs-exo ameliorated hypoxia-induced ferroptosis of neuronal cells, implying MSCs-exosomes as potential therapeutic vesicles for ASCI. Emerging evidences suggest that MSCs-exo are involved in cellular damage repair via transmitting functional non-coding RNAs. For example, MSCs-exo could transfer miR-23a-3p into the injured myocardial cells to inhibit ferroptosis [51]. Exosomal miR-140-5p released by MSCs could induce cartilaginous self-repairing in osteoarthritis rats [52]. In this study, we screened for a novel lncRNA, lncGm36569, based on the RNA sequencing of the MSCs-exosomes. lncGm36569 was enriched in ASCI mice and served as an antioxidant. Overexpression of lncGm36569 reduced ROS and iron accumulation, promoted the expression level of FSP1, and restored the functional disorder of ASCI mice, whereas reverse trends were observed in the lncGm36569-depleted group.

Increasing evidences indicate that lncRNAs function as competing ceRNAs to bind miRNAs, thus upregulating downstream target genes [53]. Using bioinformatics analysis, we confirmed that lncGm36569 harbored the binding site with miR-5627-5p. However, the role of miR-5627-5p remained unclear. Through RNA pull-down assay and luciferase reporter assay, we noted that lncGm36569 directly bound to miR-5627-5p. Overexpression of lncGm36569 reduced the level of miR-5627-5p and inhibited neuronal cell ferroptosis. Furthermore, FSP1 was elucidated to be a target of miR-5627-5p. In this work, the expression of FSP1 was upregulated after lncGm36569 transfection, while this effect was abolished when co-transfected with miR-5627-5p mimic. The effects of the lncGm36569/miR-5627-5p/

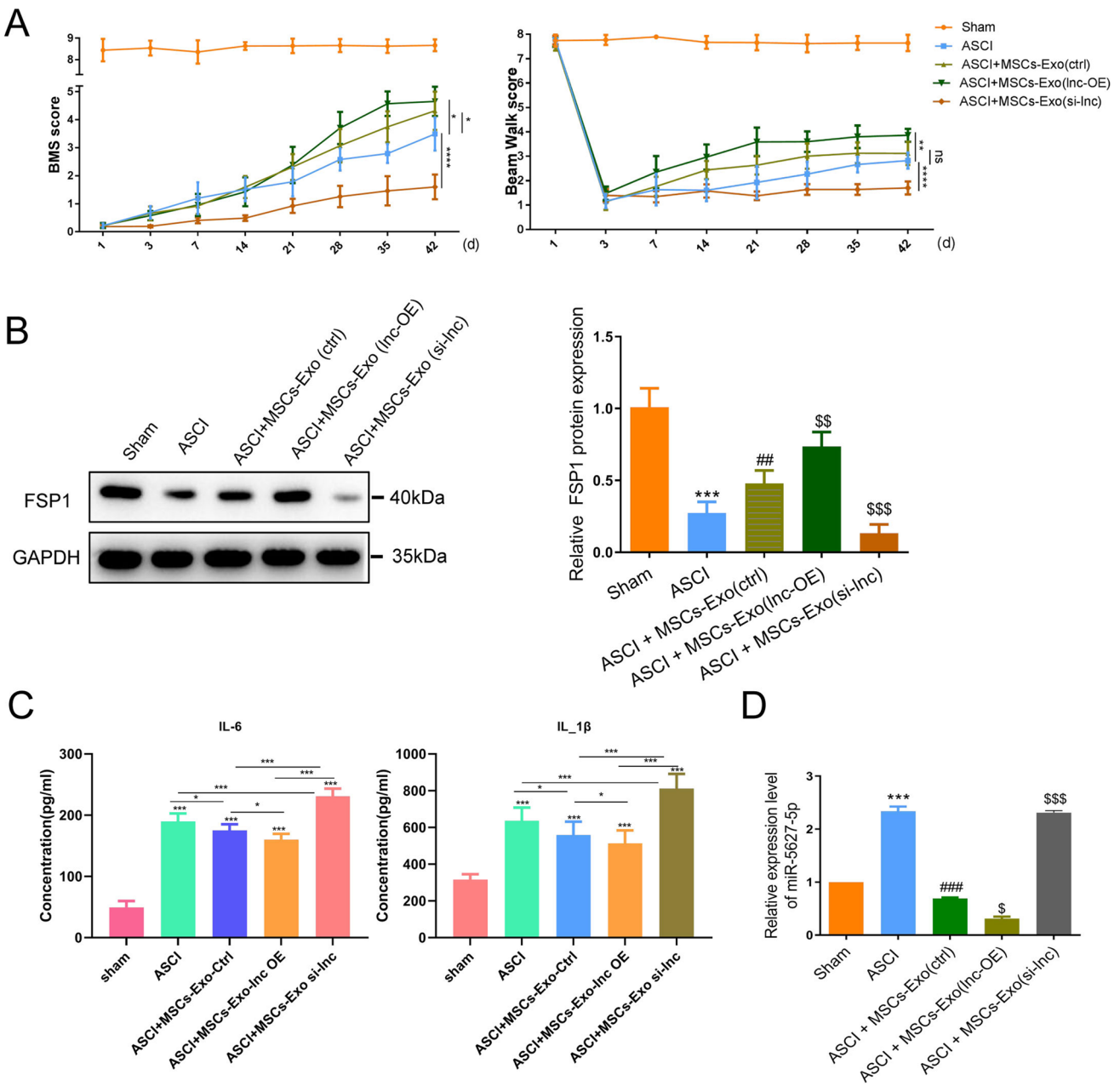

Fig. 6 Protective effects of MSCs-exo on ASCI were mediated by LncGm36569/miR-5627-5p/FSP1 axis. ASCI mouse model was established and treated by MSCs-exosomes (ctrl), MSCs-exosomes (lnc-OE) or MSCs-exosomes (si-lnc). **a** The functional disorder of the ASCI model with or without MSCs-exosomes treatments was assessed using the BMS score and beam walk score. **b** Representative blot and analyses were performed for the expression level of FSP1 in the injured spinal cord tissue after different treatments. **c** Elisa assay of inflammatory factors. **d** Real-time PCR analysis of miR-5627-5p expression in injured spinal cord tissue after different treatments. Ten animals per group, ***$p < 0.001$ vs. the sham group; ##$p < 0.01$, ###$p < 0.001$ vs. the ASCI group; \$$p < 0.05$, \$\$$p < 0.01$, \$\$\$$p < 0.001$ vs. the MSCs-exosomes (ctrl) group. Ctrl, control; lnc-OE, lncGm36569 overexpression; si-lnc, lncGm36569 knockdown; Exo, exosomes

FSP1 axis on neurological function recovery were further validated in vivo.

In summary, exosomal lncRNA Gm36569 from MSCs could facilitate neurological function repair by suppressing ferroptosis through miR-5627-5p/FSP1 axis. Our findings provided a potential therapy target for ASCI.

Authors' Contributions Chenglong Shao, and Tengyue Yang conceived the study. Chenglong Shao wrote the manuscript. Yu Chen designed the figures. Haibiao Zhao, Tengyue Yang and Yu Chen contributed to the writing and editing of the manuscript. All authors and participants reviewed the paper and approved the final manuscript.

Data Availability The data used to support the findings of this study are available from the corresponding author upon request.

Declarations

Ethics Approval and Consent to Participate All the animal experiments were approved by the Animal Ethics Committee of The First Affiliated Hospital of Zhengzhou University.

Consent for Publication Not applicable.

Competing Interests All the authors have declared no competing financial interests.

Patient Consent for Publication Not applicable.

References

1. Witiw, C. D., & Fehlings, M. G. (2015). Acute spinal cord injury. *Journal of Spinal Disorders & Techniques, 28*(6), 202–210.
2. Devivo, M. J. (2012). Epidemiology of traumatic spinal cord injury: Trends and future implications. *Spinal Cord, 50*(5), 365–372.
3. Rogers, W. K., & Todd, M. (2016). Acute spinal cord injury. *Best Practice & Research. Clinical Anaesthesiology, 30*(1), 27–39.
4. Rowland, J. W., Hawryluk, G. W., Kwon, B., & Fehlings, M. G. (2008). Current status of acute spinal cord injury pathophysiology and emerging therapies: Promise on the horizon. *Neurosurgical Focus, 25*(5), E2.
5. Berlly, M., & Shem, K. (2007). Respiratory management during the first five days after spinal cord injury. *The Journal of Spinal Cord Medicine, 30*(4), 309–318.
6. Dixon, S. J., Lemberg, K. M., Lamprecht, M. R., Skouta, R., Zaitsev, E. M., Gleason, C. E., Patel, D. N., Bauer, A. J., Cantley, A. M., Yang, W. S., et al. (2012). Ferroptosis: An iron-dependent form of nonapoptotic cell death. *Cell, 149*(5), 1060–1072.
7. Galluzzi, L., Bravo-San Pedro, J. M., Blomgren, K., & Kroemer, G. (2016). Autophagy in acute brain injury. *Nature Reviews. Neuroscience, 17*(8), 467–484.
8. Wang, Z., Zhou, L., Zheng, X., & Liu, W. (2018). Effects of dexamethasone on autophagy and apoptosis in acute spinal cord injury. *Neuroreport, 29*(13), 1084–1091.
9. Wu, F., Wei, X., Wu, Y., Kong, X., Hu, A., Tong, S., Liu, Y., Gong, F., Xie, L., Zhang, J., et al. (2018). Chloroquine promotes the recovery of acute spinal cord injury by inhibiting autophagy-associated inflammation and endoplasmic reticulum stress. *Journal of Neurotrauma, 35*(12), 1329–1344.
10. Zhang, Y., Sun, C., Zhao, C., Hao, J., Zhang, Y., Fan, B., Li, B., Duan, H., Liu, C., Kong, X., et al. (2019). Ferroptosis inhibitor SRS 16-86 attenuates ferroptosis and promotes functional recovery in contusion spinal cord injury. *Brain Research, 1706*, 48–57.
11. Choi, D. C., Lee, J. Y., Lim, E. J., Baik, H. H., Oh, T. H., & Yune, T. Y. (2012). Inhibition of ROS-induced p38MAPK and ERK activation in microglia by acupuncture relieves neuropathic pain after spinal cord injury in rats. *Experimental Neurology, 236*(2), 268–282.
12. Xiao, W., Yu, A., Liu, D., Shen, J., & Xu, Z. (2015). Ligustilide treatment promotes functional recovery in a rat model of spinal cord injury via preventing ROS production. *International Journal of Clinical and Experimental Pathology, 8*(10), 12005–12013.
13. Hao, J., Li, B., Duan, H. Q., Zhao, C. X., Zhang, Y., Sun, C., Pan, B., Liu, C., Kong, X. H., Yao, X., et al. (2017). Mechanisms underlying the promotion of functional recovery by deferoxamine after spinal cord injury in rats. *Neural Regeneration Research, 12*(6), 959–968.
14. Imai, H., Matsuoka, M., Kumagai, T., Sakamoto, T., & Koumura, T. (2017). Lipid peroxidation-dependent cell death regulated by GPx4 and Ferroptosis. *Current Topics in Microbiology and Immunology, 403*, 143–170.
15. Zhou, H., Yin, C., Zhang, Z., Tang, H., Shen, W., Zha, X., Gao, M., Sun, J., Xu, X., & Chen, Q. (2020). Proanthocyanidin promotes functional recovery of spinal cord injury via inhibiting ferroptosis. *Journal of Chemical Neuroanatomy, 107*, 101807.
16. Yao, X., Zhang, Y., Hao, J., Duan, H. Q., Zhao, C. X., Sun, C., Li, B., Fan, B. Y., Wang, X., Li, W. X., et al. (2019). Deferoxamine promotes recovery of traumatic spinal cord injury by inhibiting ferroptosis. *Neural Regeneration Research, 14*(3), 532–541.
17. Sykova, E., Jendelova, P., Urdzikova, L., Lesny, P., & Hejcl, A. (2006). Bone marrow stem cells and polymer hydrogels--two strategies for spinal cord injury repair. *Cellular and Molecular Neurobiology, 26*(7–8), 1113–1129.
18. Oshigiri, T., Sasaki, T., Sasaki, M., Kataoka-Sasaki, Y., Nakazaki, M., Oka, S., Morita, T., Hirota, R., Yoshimoto, M., Yamashita, T., et al. (2019). Intravenous infusion of mesenchymal stem cells alters motor cortex gene expression in a rat model of acute spinal cord injury. *Journal of Neurotrauma, 36*(3), 411–420.
19. Kim, Y. C., Kim, Y. H., Kim, J. W., & Ha, K. Y. (2016). Transplantation of mesenchymal stem cells for acute spinal cord injury in rats: Comparative study between Intralesional injection and scaffold based transplantation. *Journal of Korean Medical Science, 31*(9), 1373–1382.
20. Jin, M. C., Medress, Z. A., Azad, T. D., Doulames, V. M., & Veeravagu, A. (2019). Stem cell therapies for acute spinal cord injury in humans: A review. *Neurosurgical Focus, 46*(3), E10.
21. Kim, C., Kim, H. J., Lee, H., Lee, H., Lee, S. J., Lee, S. T., Yang, S. R., & Chung, C. K. (2019). Mesenchymal stem cell transplantation promotes functional recovery through MMP2/STAT3 related Astrogliosis after spinal cord injury. *International Journal of Stem Cells, 12*(2), 331–339.
22. Liu, W., Wang, Y., Gong, F., Rong, Y., Luo, Y., Tang, P., Zhou, Z., Zhou, Z., Xu, T., Jiang, T., et al. (2019). Exosomes derived from bone mesenchymal stem cells repair traumatic spinal cord injury by suppressing the activation of A1 neurotoxic reactive astrocytes. *Journal of Neurotrauma, 36*(3), 469–484.
23. Romanelli, P., Bieler, L., Scharler, C., Pachler, K., Kreutzer, C., Zaunmair, P., Jakubecova, D., Mrowetz, H., Benedetti, B., Rivera, F. J., et al. (2019). Extracellular vesicles can deliver anti-inflammatory and anti-scarring activities of mesenchymal stromal cells after spinal cord injury. *Frontiers in Neurology, 10*, 1225.
24. Ruppert, K. A., Nguyen, T. T., Prabhakara, K. S., Toledano Furman, N. E., Srivastava, A. K., Harting, M. T., Cox Jr., C. S., & Olson, S. D. (2018). Human mesenchymal stromal cell-derived extracellular vesicles modify microglial response and improve clinical outcomes in experimental spinal cord injury. *Scientific Reports, 8*(1), 480.
25. Thery, C., Zitvogel, L., & Amigorena, S. (2002). Exosomes: Composition, biogenesis and function. *Nature Reviews. Immunology, 2*(8), 569–579.

26. Ela, S., Mager, I., Breakefield, X. O., & Wood, M. J. (2013). Extracellular vesicles: Biology and emerging therapeutic opportunities. *Nature Reviews. Drug Discovery, 12*(5), 347–357.
27. Chen, L. L., & Zhao, J. C. (2014). Functional analysis of long noncoding RNAs in development and disease. *Advances in Experimental Medicine and Biology, 825*, 129–158.
28. Mao, C., Wang, X., Liu, Y., Wang, M., Yan, B., Jiang, Y., Shi, Y., Shen, Y., Liu, X., Lai, W., et al. (2018). A G3BP1-interacting lncRNA promotes Ferroptosis and apoptosis in Cancer via nuclear sequestration of p53. *Cancer Research, 78*(13), 3484–3496.
29. Wang, M., Mao, C., Ouyang, L., Liu, Y., Lai, W., Liu, N., Shi, Y., Chen, L., Xiao, D., Yu, F., et al. (2019). Long noncoding RNA LINC00336 inhibits ferroptosis in lung cancer by functioning as a competing endogenous RNA. *Cell Death and Differentiation, 26*(11), 2329–2343.
30. Yang, Y., Tai, W., Lu, N., Li, T., Liu, Y., Wu, W., Li, Z., Pu, L., Zhao, X., Zhang, T., et al. (2020). lncRNA ZFAS1 promotes lung fibroblast-to-myofibroblast transition and ferroptosis via functioning as a ceRNA through miR-150-5p/SLC38A1 axis. *Aging (Albany NY), 12*(10), 9085–9102.
31. Wu, Y., Zhang, S., Gong, X., Tam, S., Xiao, D., Liu, S., & Tao, Y. (2020). The epigenetic regulators and metabolic changes in ferroptosis-associated cancer progression. *Molecular Cancer, 19*(1), 39.
32. Koozekanani, S. H., Vise, W. M., Hashemi, R. M., & Mcghee, R. B. (1976). Possible mechanisms for observed pathophysiological variability in experimental spinal cord injury by the method of Allen. *Journal of Neurosurgery, 44*(4), 429.
33. Mammana, S., Gugliandolo, A., Cavalli, E., Diomede, F., Iori, R., Zappacosta, R., Bramanti, P., Conti, P., Fontana, A., Pizzicannella, J. (2019). Human gingival mesenchymal stem cells pretreated with vesicular moringin nanostructures as a new therapeutic approach in a mouse model of spinal cord injury. *Wiley-Blackwell Online Open, 13*(7).
34. Wei, L, Yongxiang, W., Fangyi, G., Yuluo, R., Yongjun, L., Pengyu, T., Zheng, Z., Zhimin, Z., Tao, X., Tao, J. (2018). Exosomes derived from bone mesenchymal stem cells repair traumatic spinal cord injury via suppressing the activation of A1 neurotoxic reactive astrocytes. *Journal of Neurotrauma*: neu.2018.5835-.
35. Sedy, J., Urdzikova, L., Jendelova, P., & Sykova, E. (2008). Methods for behavioral testing of spinal cord injured rats. *Neuroscience and Biobehavioral Reviews, 32*(3), 550–580.
36. Basso, D. M., Fisher, L. C., Anderson, A. J., Jakeman, L. B., Mctigue, D. M., & Popovich, P. G. (2006). Basso mouse scale for locomotion detects differences in recovery after spinal cord injury in five common mouse strains. *Journal of Neurotrauma, 23*(5), 635.
37. Asadi-Golshan, R., Razban, V., Mirzaei, E., Rahmanian, A., Khajeh, S., Mostafavi-Pour, Z., & Dehghani, F. (2018). Sensory and motor behavior evidences supporting the usefulness of conditioned medium from dental pulp-derived stem cells in spinal cord injury in rats. *Asian Spine J, 12*(5), 785–793.
38. von Euler, M., Akesson, E., Samuelsson, E. B., Seiger, A., & Sundstrom, E. (1996). Motor performance score: A new algorithm for accurate behavioral testing of spinal cord injury in rats. *Experimental Neurology, 137*(2), 242–254.
39. Thery, C., Amigorena, S., Raposo, G., Clayton, A. (2006). Isolation and characterization of exosomes from cell culture supernatants and biological fluids. *Current Protocols in Cell Biology*, Chapter 3:Unit 3 22.
40. Lu, K., Li, H. Y., Yang, K., Wu, J. L., Cai, X. W., Zhou, Y., & Li, C. Q. (2017). Exosomes as potential alternatives to stem cell therapy for intervertebral disc degeneration: In-vitro study on exosomes in interaction of nucleus pulposus cells and bone marrow mesenchymal stem cells. *Stem Cell Research & Therapy, 8*(1), 108.
41. Liu, Z., Wang, H., Cai, H., Hong, Y., Li, Y., Su, D., & Fan, Z. (2018). Long non-coding RNA MIAT promotes growth and metastasis of colorectal cancer cells through regulation of miR-132/Derlin-1 pathway. *Cancer Cell International, 18*, 59.
42. Wang, W. T., Ye, H., Wei, P. P., Han, B. W., He, B., Chen, Z. H., & Chen, Y. Q. (2016). LncRNAs H19 and HULC, activated by oxidative stress, promote cell migration and invasion in cholangiocarcinoma through a ceRNA manner. *Journal of Hematology & Oncology, 9*(1), 117.
43. Chen, G., Guo, G., Zhou, X., & Chen, H. (2020). Potential mechanism of ferroptosis in pancreatic cancer. *Oncology Letters, 19*(1), 579–587.
44. Wei, X., Yi, X., Zhu, X. H., & Jiang, D. S. (2020). Posttranslational modifications in Ferroptosis. *Oxidative Medicine and Cellular Longevity, 2020*, 8832043.
45. Tian, Y., Lu, J., Hao, X., Li, H., Zhang, G., Liu, X., Li, X., Zhao, C., Kuang, W., Chen, D., & Zhu, M. (2020). FTH1 inhibits Ferroptosis through Ferritinophagy in the 6-OHDA model of Parkinson's disease. *Neurotherapeutics, 17*(4), 1796–1812.
46. Cheng, J., Fan, Y. Q., Liu, B. H., Zhou, H., Wang, J. M., & Chen, Q. X. (2020). ACSL4 suppresses glioma cells proliferation via activating ferroptosis. *Oncology Reports, 43*(1), 147–158.
47. Song, X., & Long, D. (2020). Nrf2 and Ferroptosis: A new research direction for neurodegenerative diseases. *Frontiers in Neuroscience, 14*, 267.
48. Li, Y., Wang, J., Chen, S., Wu, P., Xu, S., Wang, C., Shi, H., & Bihl, J. (2020). miR-137 boosts the neuroprotective effect of endothelial progenitor cell-derived exosomes in oxyhemoglobin-treated SH-SY5Y cells partially via COX2/PGE2 pathway. *Stem Cell Research & Therapy, 11*(1), 330.
49. Bersuker, K., Hendricks, J. M., Li, Z., Magtanong, L., Ford, B., Tang, P. H., Roberts, M. A., Tong, B., Maimone, T. J., Zoncu, R., et al. (2019). The CoQ oxidoreductase FSP1 acts parallel to GPX4 to inhibit ferroptosis. *Nature, 575*(7784), 688–692.
50. Chen, L., & Xie, J. (2020). Ferroptosis-suppressor-protein 1: A potential neuroprotective target for combating Ferroptosis. *Movement Disorders, 35*(3), 400.
51. Song, Y., Wang, B., Zhu, X., Hu, J., Sun, J., Xuan, J., & Ge, Z. (2020). Human umbilical cord blood-derived MSCs exosome attenuate myocardial injury by inhibiting ferroptosis in acute myocardial infarction mice. *Cell Biology and Toxicology*.
52. Geng, Y., Chen, J., Alahdal, M., Chang, C., Duan, L., Zhu, W., Mou, L., Xiong, J., Wang, M., & Wang, D. (2020). Intra-articular injection of hUC-MSCs expressing miR-140-5p induces cartilage self-repairing in the rat osteoarthritis. *Journal of Bone and Mineral Metabolism, 38*(3), 277–288.
53. Thomson, D. W., & Dinger, M. E. (2016). Endogenous microRNA sponges: Evidence and controversy. *Nature Reviews. Genetics, 17*(5), 272–283.

Publisher's Note Springer Nature remains neutral with regard to jurisdictional claims in published maps and institutional affiliations.